The DCX-domain tandems of doublecortin and doublecortin-like kinase

Myung Hee Kim[1,2], Tomasz Cierpicki[1–3], Urszula Derewenda[1,2], Daniel Krowarsch[3], Yuanyi Feng[4], Yancho Devedjiev[2], Zbigniew Dauter[5], Christopher A. Walsh[4], Jacek Otlewski[2,3], John H. Bushweller[2] and Zygmunt S. Derewenda[2]

Published online 14 April 2003; doi:10.1038/nsb918

The doublecortin-like domains (DCX), which typically occur in tandem, are novel microtubule-binding modules. DCX tandems are found in doublecortin, a 360-residue protein expressed in migrating neurons; the doublecortin-like kinase (DCLK); the product of the *RP1* gene that is responsible for a form of inherited blindness; and several other proteins. Mutations in the gene encoding doublecortin cause lissencephaly in males and the 'double-cortex syndrome' in females. We here report a solution structure of the N-terminal DCX domain of human doublecortin and a 1.5 Å resolution crystal structure of the equivalent domain from human DCLK. Both show a stable, ubiquitin-like tertiary fold with distinct structural similarities to GTPase-binding domains. We also show that the C-terminal DCX domains of both proteins are only partially folded. In functional assays, the N-terminal DCX domain of doublecortin binds only to assembled microtubules, whereas the C-terminal domain binds to both microtubules and unpolymerized tubulin.

Microtubules are key components of cytoskeleton that are involved in cell movement, shape determination, division and transport[1]. Microtubule-associated proteins (MAPs) regulate the dynamics and distribution of microtubules by binding in a nucleotide-independent manner[2]. MAPs are particularly vital to neurons, where they regulate embryonic neuronal migration, as well as growth of dendrites and axons. Recently, a novel gene, *DCX*, coding for a microtubule-associated protein was identified on chromosome X[3,4]. The protein encoded by this gene, doublecortin, is essential for proper embryonic development of the layers of the cerebral cortex, formed by neurons migrating from specialized regions deep within the brain in an 'inside-out' pattern. The later born neuron cells migrate over progressively longer distances past the neuronal layers formed earlier, often in excess of 1,000 cell lengths, to reach their destination. Mutations in the *DCX* gene cause a syndrome resulting in X-linked lissencephaly (XLIS), or 'smooth-brain', in males. Females that are heterozygous for the X-linked mutations suffer from a milder version of this syndrome, with a subpopulation of neurons arrested approximately halfway before reaching the expected destination during cerebral cortex development, producing so-called subcortical band heterotopia (SBH) or 'double-cortex'[3–7]. In surviving patients, this syndrome leads to severe retardation and seizures[8,9]. The doublecortin protein is 40 kDa in size and has an amino acid sequence unique among known MAPs.

The mapping of pathogenic mutations identified a tandem of two homologous domains within doublecortin, spanning approximately residues 47–135 and 174–259 (refs. 10,11). Similar tandems are found in other proteins, one of which is the evolutionarily conserved doublecortin-like kinase, DCLK[12–14], which harbors a Ser/Thr kinase domain downstream of the tandem. (The protein doublecortin and the doublecortin-like domains are all denoted in literature and in the SMART database[15] as DCX. Here, we use DCX to describe the generic domain, the term doublecortin describes the full length protein, N-DCX and C-DCX describe the N- and C-terminal DCX domains within doublecortin, respectively, and N-DCLK and C-DCLK describe the two DCX domains within DCLK.) Although the physiological function of the human DCLK is not clear, the *Caenorhabditis elegans* homolog of DCLK, ZYG-8, promotes microtubule assembly during embryonic anaphase, binds to microtubules and stabilizes them[16]. Another example of a DCX-containing protein is *retinitis pigmentosa* RP1 protein, which is mutated in 5–10% of cases of autosomal dominant retinopathy[17]. The disease is a form of night blindness that may lead to complete lack of vision.

Here we report the solution structure of the N-terminal DCX domain of human doublecortin and the 1.5 Å crystal structure of analogous domain of DCLK. The domain has a novel fold among MAPs but one that is well known among GTPase-binding domains and ubiquitin-related proteins. We also show that the C-terminal DCX domains of DCLK and doublecortin are only partially folded. Finally, we present evidence that each of the two DCX domains of doublecortin interacts with tubulin and microtubules in a different way, suggesting a general mechanism by which the DCX-tandems function in MAPs.

The solution structure of the N-DCX

Repeated experiments aimed at the preparation of X-ray–quality crystals of the recombinant full-length doublecortin, its DCX-tandem or individual DCX domains have failed. Therefore, we used heteronuclear NMR to characterize the solution structure of the N-DCX (residues 45–150). The sequential assignment of the ^{15}N,^{13}C-enriched, recombinant

[1]The contributions of these authors were particularly important to this study. [2]Department of Molecular Physiology and Biological Physics, University of Virginia, Charlottesville, Virginia 22908-0736, USA. [3]Laboratory of Protein Engineering, Institute of Biochemistry & Molecular Biology, University of Wroclaw, Tamka 2, 50-137 Wroclaw, Poland. [4]Division of Neurogenetics, Department of Neurology, Beth Israel Deaconess Medical Center, Boston, Massachusetts 02115, USA. [5]Synchrotron Radiation Research Section, Macromolecular Crystallography Laboratory, NCI, Brookhaven National Laboratory, Upton, New York 11973, USA.

Correspondence should be addressed to Z.S.D. *e-mail: zsd4n@virginia.edu* or J.H.B. *e-mail: jhb4v@virginia.edu*

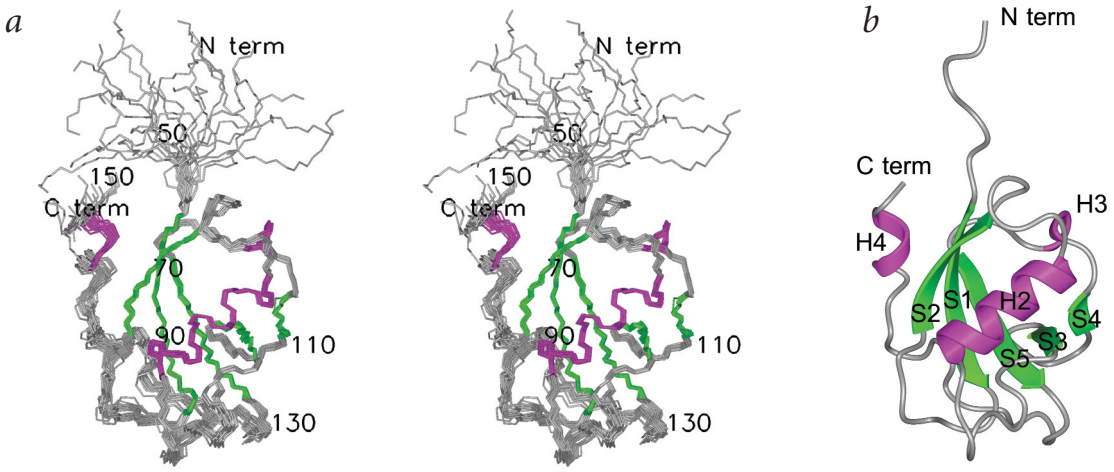

Fig. 1 Solution structure of the N-terminal DCX domain of human doublecortin. ***a***, Stereo view of the 20 lowest-energy structures with every 20th residue labeled. ***b***, Representative conformation of N-DCX in ribbon representation. The β-strands (green) and α-helices (magenta) are labeled.

protein is described elsewhere[18]. The structure was determined from a total of 1,692 distance restraints (Table 1; Fig. 1). A well-defined core comprising residues 51–147 is observed, with the N and C termini displaying disorder in the structure, as confirmed by measurements of the ^{1}H-^{15}N–heteronuclear NOE (data not shown). The core folds into a single compact domain with a mixed β-sheet containing five β-strands arranged in the order 2-1-5-3-4. There is a single major α-helix (residues 80–91) within the crossover connection between strands β2 and β3. This helix fits onto the concave face of the β-sheet. There are two 3_{10}-helices that comprise fragments 116–118 and 145–148. For residues beyond position 141, decreasing values of the ^{1}H-^{15}N heteronuclear NOEs were observed — that is, 0.4–0.6 relative to a mean value of 0.74 for the well-defined core — indicative of an increased degree of mobility. Despite the increased mobility, several long-range NOEs are observed between the side chain of Trp147 and residues that are part of the domain core (for example, Arg56, Val69 and Gly122), demonstrating that the C terminus is partly anchored in the protein core in solution. To evaluate the importance of the N-DCX C terminus for proper folding, we constructed a deletion mutant in which residues beyond 141 were removed. Examination of ^{1}H-^{15}N HSQC spectra using ^{15}N-labeled samples showed that, with the exception of chemical shifts associated with residues interacting with the C terminus, the spectra are identical to the wild type protein (data not shown).

The crystal structure of the N-DCLK

The crystal structure of N-DCLK was solved in a semi-automated manner using the anomalous signal from a single Se atom in a selenomethionine (SeMet)-substituted sample of a mutant protein, in which Leu120 was replaced with a Met (L120M), which occurs in this position in doublecortin, and refined to 1.6 Å resolution. A crystal of wild type N-DCLK that lacks methionines was also grown, and the structure — virtually identical to the mutant — was refined to 1.5 Å resolution (Table 2; Fig. 2). All residues between Thr49 and Val154 are visible in the electron density map.

The N-DCLK contains a single mixed β-sheet containing five β-strands and a single major α-helix (residues 84–95), which binds in the concave groove of the β-sheet. There are three short 3_{10}-helices: residues 53–55, 120–122 and 148–151. In general terms, the tertiary structure of N-DCLK compares well with the NMR structure of the equivalent domain in doublecortin, except for the region extending from the end of strand β5 (residue 134) to the C terminus. In both the NMR and crystal structures, these fragments have similar conformations but are shifted by ~2 Å with respect to one another. In N-DCLK, the C-terminal fragment is involved in close crystal contacts, which can easily stabilize one specific conformation.

Similarity to GTPase-binding domains

A Dali[19] search with the coordinates of N-DCX and N-DCLK indicated that the DCX domain shows distinct structural simi-

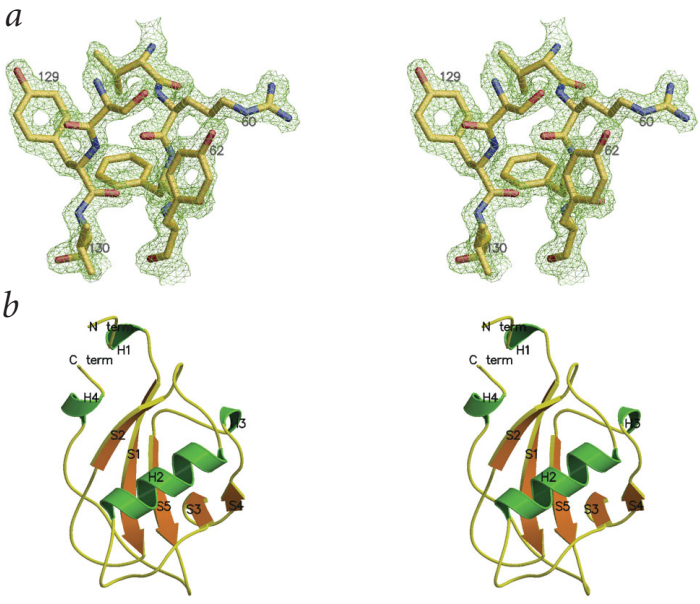

Fig. 2 The crystal structure of the N-terminal DCX domain of the doublecortin-like kinase. ***a***, Stereo view of representative $2F_o - F_c$ electron density contoured at 1.4 σ. ***b***, Stereo view of secondary structure elements of N-DCLK, as defined by PROCHECK[54]. The view is identical to the one in Fig. 1.

larities to the Ras-binding domain of RalGDS[20], the PB1 domain of Bem1p[21,22], the UBX domain of human FAF1 (ref. 23) and ubiquitin[24] — all members of the ubiquitin-like superfamily (Fig. 3). Other GTPase-binding domains, including that of Byr2 (ref. 25), are also similar in their overall three-dimensional structure. There is no evidence from amino acid sequence similarity that would suggest common ancestry for these proteins, but the possibility cannot be excluded. It should be noted that tubulin is also a GTPase, and the structural similarities between the two systems may extend to their function.

Similarities in amino acid sequence between the N- and C-terminal DCX domains in proteins containing the DCX tandems (Fig. 3*d*) suggest that the two domains should show a common three-dimensional fold. Thus, the DCX domains constitute the first known example of a microtubule-interacting module with a canonical ubiquitin fold. A comparison of other members of this structural superfamily with DCX reveals that the general ββαβββ topology is consistently preserved, although the C termini may vary among the different proteins (Fig. 3*a–c*).

Stability of N- and C-terminal DCX domains

We found that the recombinant C-terminal DCX domains of both doublecortin and DCLK are thermodynamically unstable. Neither shows cooperative unfolding in temperature– or guanidine-HCl–induced denaturation experiments, whereas the size exclusion analysis shows a profile with a predominant monomeric fraction in equilibrium with oligomers (data not shown). The measured Stokes radius (R_s) of each C-terminal DCX domain is ~20.4 Å, which is too large for a folded monomeric species but consistent with a value predicted for molten globule[26]. In contrast, the N-terminal DCX domains of both doublecortin and DCLK show cooperative and reversible temperature-induced denaturation, with relatively high denaturation temperatures (T_{den}) of 70.6 °C and 73.8 °C, respectively. The values of ΔG_{den} determined by guanidine-HCl unfolding for doublecortin and DCLK are 4.2 kcal mol^{-1} and 6.6 kcal mol^{-1}, respectively (Fig. 4*a*). In contrast to the C-terminal DCX domains, the R_s values of N-terminal domains are 16.2 Å for doublecortin and 18.9 Å for DCLK, in good agreement with the values calculated for globular proteins of this size[26].

The DCX tandems show more complex behavior, with chemical denaturation profiles deviating slightly from a two-state model (Fig. 4*a*). The apparent T_{den} of the DCX tandem of doublecortin is 64.9 °C, whereas the DCX-tandem of DCLK precipitates at higher temperatures, precluding determination of melting temperature.

To further investigate the structure of C-terminal DCX domains, we used 8-anilino-1-naphthalene sulfonate (ANS), a probe widely used to study partially folded and molten globule states[27–29]. In an aqueous environment, the fluorescence of this dye is quenched; however, when in contact with hydrophobic

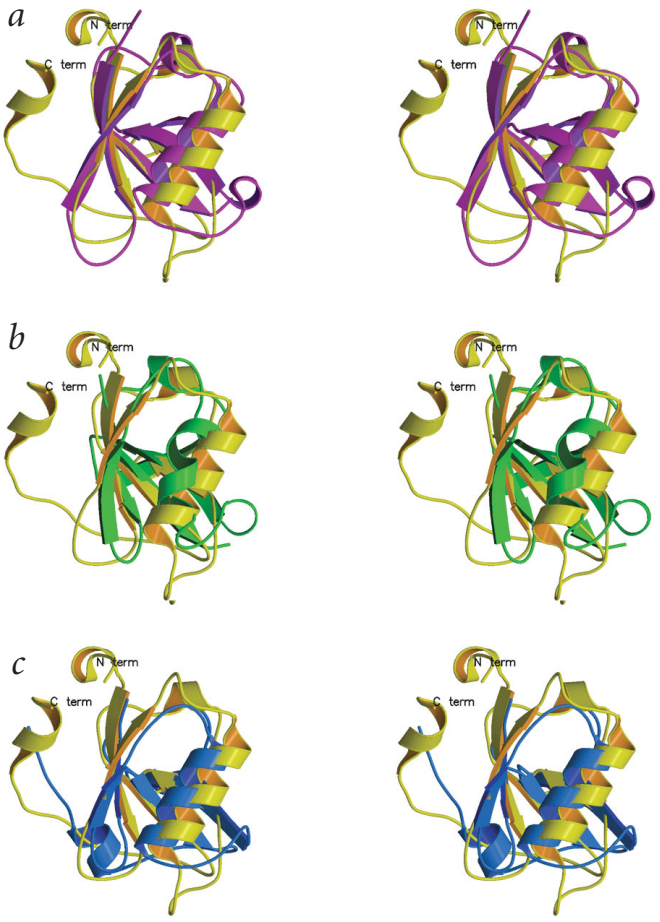

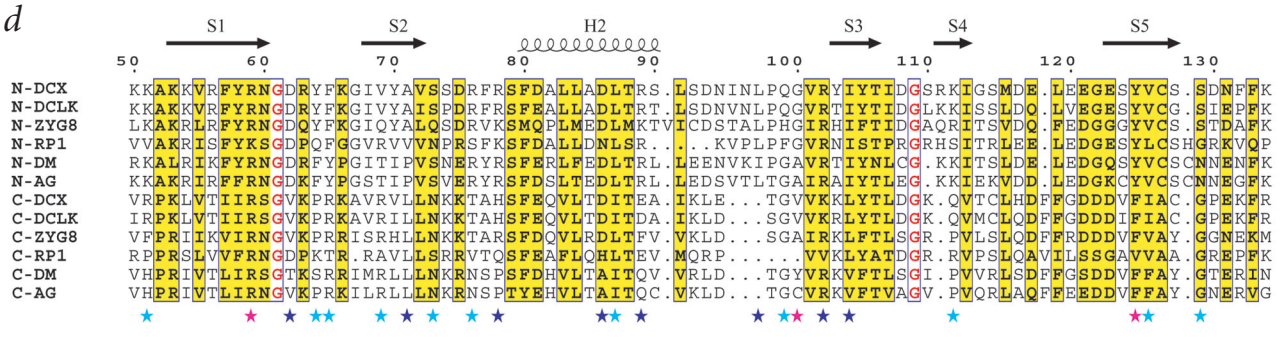

Fig. 3 Comparison of molecular models of structurally related members of the ubiquitin superfamily. Stereo views of the crystal structure of the N-DCLK domain (yellow/orange) compared with the structures of ***a***, RalGDS Ras-binding domain (PDB entry 1LFD; magenta); ***b***, the structure of Byr2 Ras-binding domain (1K8R; green); and ***c***, C-Raf1 Ras-binding domain (1GUA; blue). ***d***, Sequence alignment of the N-terminal domain of doublecortin (N-DCX) with other DCX-like domains, including those of doublecortin-like kinase (N-DCLK), *C. elegans* zyg-8 (N-ZYG8), the human RP1 (N-RP1), *Drosophila melanogaster* homolog (N-DM), *Anopheles gambiae* homolog (AG) and with their respective C-terminal domains. The secondary structure elements and sequence numbering are based on the N-DCX structure. Blue stars denote sites of mutations in N-DCX occurring in patients with XLIS and SBH, cyan stars show corresponding sites in C-DCX and magenta stars indicate sites common to both domains.

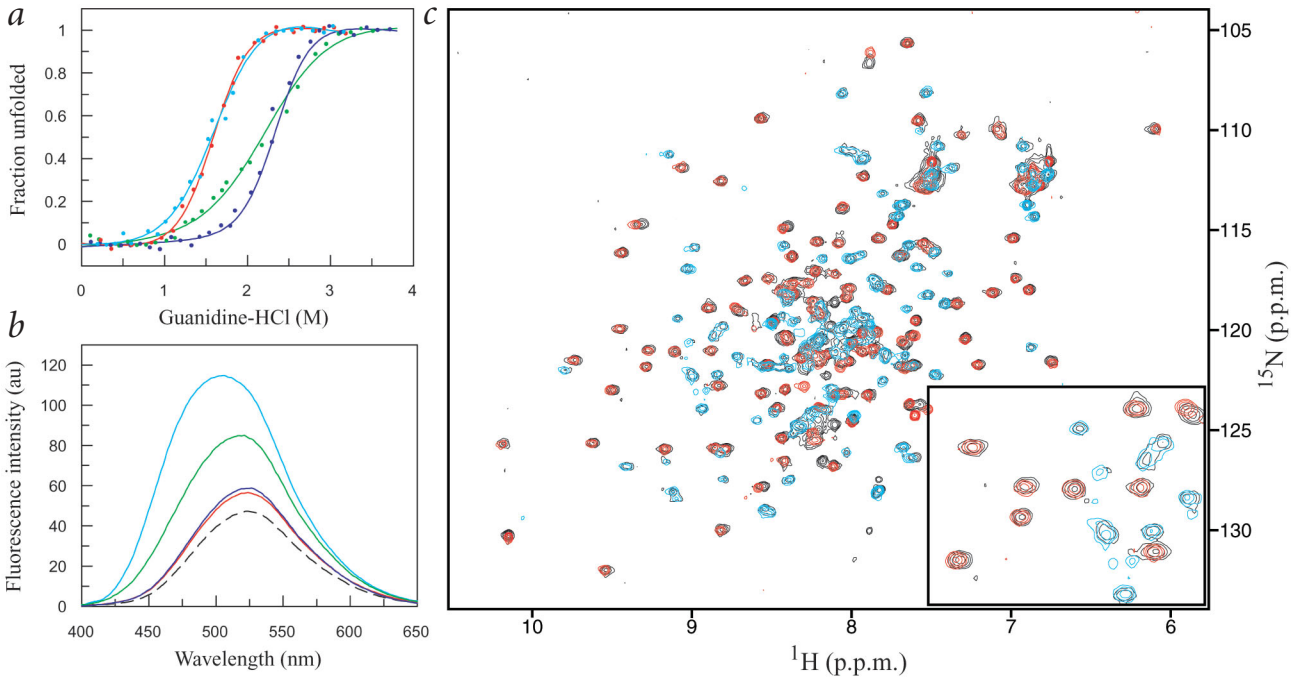

Fig. 4 Comparison of the stabilities of the isolated DCX domains and DCX tandems in doublecortin and DCLK. ***a***, Stability properties of DCX tandems and respective isolated N-terminal DCX domains. Guanidine-HCl denaturation of N-DCX of doublecortin (red), DCX tandem of doublecortin (cyan), N-DCLK (blue) and DCX tandem of DCLK (green) monitored by changes in CD signal at 220 nm. ***b***, ANS binding to isolated N- and C-terminal DCX domains of doublecortin and DCLK. Fluorescence spectra of ANS in presence of N-DCX of doublecortin (red), N-DCLK (blue), C-DCX of doublecortin (cyan) and C-DCLK (green). All spectra were recorded at protein concentration 9×10^{-6} M. Free ANS fluorescence is also shown (dashed black line). ***c***, ^{1}H-^{15}N HSQC spectra of N-DCX (red) and C-DCX (cyan) superimposed onto DCX tandem (black). Spectra were recorded at a concentration of 60 μM at 20 °C and pH 6.8. Inset shows expanded fragment of the spectra emphasizing difference between the linewidths of N-DCX and C-DCX.

surfaces exposed in molten globules or found in non-polar binding sites of some folded proteins, the intensity is significantly enhanced. We find that ANS binds to both C-terminal DCX domains with an intensity increase accompanied by a significant shift toward a shorter wavelength at 9×10^{-6} M protein concentration (Fig. 4*b*). A similar effect is observed for DCX tandems. No ANS binding was detected for the N-terminal DCX domains.

Attempts to obtain NMR spectra of C-DCX at 200 μM protein concentration failed because of aggregation problems; however, at 60 μM, the ^{1}H-^{15}N HSQC spectrum was reasonably well dispersed, although significant line-broadening was still observed (Fig. 4*c*). The signals are likely to be broadened primarily because of conformational disorder and conformational exchange on a millisecond timescale[30]. A similar effect was observed for locally disordered conformers upon pressure-induced unfolding of apomyoglobin[31]. This residual structure made it possible for us to study the behavior of C-DCX in the presence of tubulin (see below), although the low protein concentration in the sample has prevented us, so far, from a more detailed structural characterization.

The DCX tandem of doublecortin

One of the possible reasons for the properties of isolated C-DCX could be the stabilizing interaction with N-DCX in the tandem. We have therefore explored the properties of the intact DCX tandem (residues 45–275). The ^{1}H-^{15}N HSQC spectra at 60 μM and 200 μM protein concentration showed significant concentration-dependent broadening of signals from the C-terminal DCX domain while signals of the N-terminal domain were virtually unaffected. The presence of a covalently linked, well-folded N-terminal domain reduces the tendency of C-DCX to aggregate. In the HSQC spectra of DCX tandem compared with isolated N-DCX and C-DCX (Fig. 4*c*), the signal lines corresponding to N-DCX were marginally broader relative to the isolated domain, with no changes in chemical shifts. This is consistent with a small increase in the correlation time of N-DCX domain in tandem, because of a higher molecular weight, without any conformational changes induced by C-DCX. In addition, the chemical shifts of C-DCX in tandem are almost unperturbed relatively to isolated domain. Finally, we conducted experiments involving titration of ^{15}N-labeled N-DCX domain with unlabeled C-DCX (data not shown). We did not observe any chemical shift perturbations and conclude that the two domains within the tandem do not interact in any significant way other than through a covalent, flexible linker region. The molecular causes underlying the partial folding of the C-terminal DCX domains are now under investigation in our laboratories.

Binding of N- and C-DCX to tubulin

Previous work established that doublecortin and DCLK co-localize with the microtubule cytoskeleton and stabilize microtubules[32,33], but the pattern of binding of the isolated DCX domains to the elements of the microtubule cytoskeleton remained uncertain. We used biotinylated tubulin in pull-down experiments using resin-bound avidin to examine the tubulin-binding properties of doublecortin and its DCX domains. Four constructs were used: the full-length protein, the DCX tandem, N-DCX and C-DCX. When the biotinylated, unpolymerized dimeric tubulin was captured and pelleted by the avidin-resin, the pellet, as well as the supernatant, was examined for the presence of DCX-derived constructs with polyclonal antibodies to

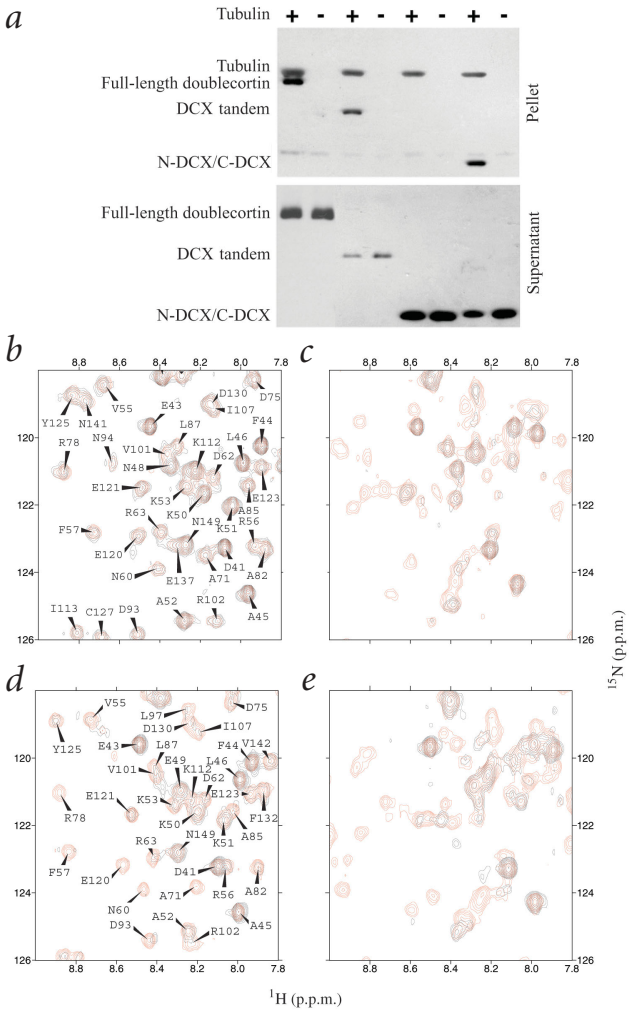

Fig. 5 Binding of doublecortin DCX domains to tubulin. ***a***, *In vitro* pull-down assay of the different doublecortin constructs with tubulin.The experiments contain, from left to right, full length doublecortin, DCX-tandem, N-DCX and C-DCX, with (+) and without (–) tubulin. The top and bottom panels show the pellet and the supernatant, respectively. ***b***, ^{1}H-^{15}N HSQC spectra of 60 μM N-DCX in the presence (black) and absence (red) of equimolar dimeric tubulin at 20 °C. ***c***, ^{1}H-^{15}N HSQC spectra of 60 μM C-DCX in the presence (black) and absence (red) of equimolar dimeric tubulin at 20 °C. ***d***, ^{1}H-^{15}N HSQC spectra of 60 μM N-DCX in the presence (black) and absence (red) of equimolar polymerized tubulin at 35 °C. ***e***, ^{1}H-^{15}N HSQC spectra of 60 μM C-DCX in the presence (black) and absence (red) of equimolar polymerized tubulin at 35 °C.

doublecortin and tubulin. All constructs, except for the N-DCX domain, were present in the pellet, whereas the supernatant contained all proteins (Fig. 5*a*). Thus, N-DCX alone is incapable of binding to dimeric, soluble tubulin.

In an independent series of experiments, we monitored tubulin- and microtubule-binding of various doublecortin constructs using NMR. To assess the ability of the isolated domains of doublecortin to bind to polymerized tubulin, we exploited the temperature-dependent behavior of tubulin, which at 60 μM concentration and 20 °C exists predominantly as dimer but tends to polymerize rapidly at 35 °C because of spontaneous nucleation[34,35]. When the temperature is increased to 35 °C, the sample shows increased turbidity, and the effect is reversible.

First, we measured the ^{1}H-^{15}N HSQC spectra of ^{15}N-labeled doublecortin fragments in the presence of unlabeled tubulin at a 1:1 molar ratio (per tubulin dimer). Although a physiological ratio of doublecortin to tubulin is estimated to be ~1:70 (ref. 11), the highest rate of tubulin polymerization occurs when the concentrations are equimolar[32]. The high molecular weight of the tubulin dimer (110 kDa) allowed us to use the observed binding-associated signal broadening in ^{1}H-^{15}N HSQC spectra as an indicator of intermolecular interactions. Repeated experiments conducted at 20 °C showed that the signals of N-DCX are virtually identical, regardless of whether or not tubulin was present (Fig. 5*b*). However, the spectrum recorded for the C-DCX domain in the presence of tubulin shows substantial signal broadening of resonances, consistent with the binding of the C-DCX domain to unpolymerized tubulin (Fig. 5*c*).

In NMR experiments conducted with samples at 35 °C, the ^{1}H-^{15}N HSQC spectra show substantial broadening of resonances for both domains, consistent with binding to microtubules by both domains (Fig. 5*d*,*e*). For the N-terminal DCX domain, lowering the temperature back to 20 °C (microtubule depolymerization) resulted in the recovery of the spectrum characteristic of unbound protein. In contrast, lowering the temperature for the C-terminal DCX domain resulted only in small temperature-induced chemical shift changes but no change in the broadening-induced loss of resonances. We considered the possibility that the observed broadening effects are due to changes in viscosity associated with tubulin polymerization, but subsequent study of the R89G mutant of N-DCX (see discussion below) ruled this out.

Finally, to verify the impact of isolated DCX domains on the polymerization rate of tubulin at the 1:1 molar ratio (as used in

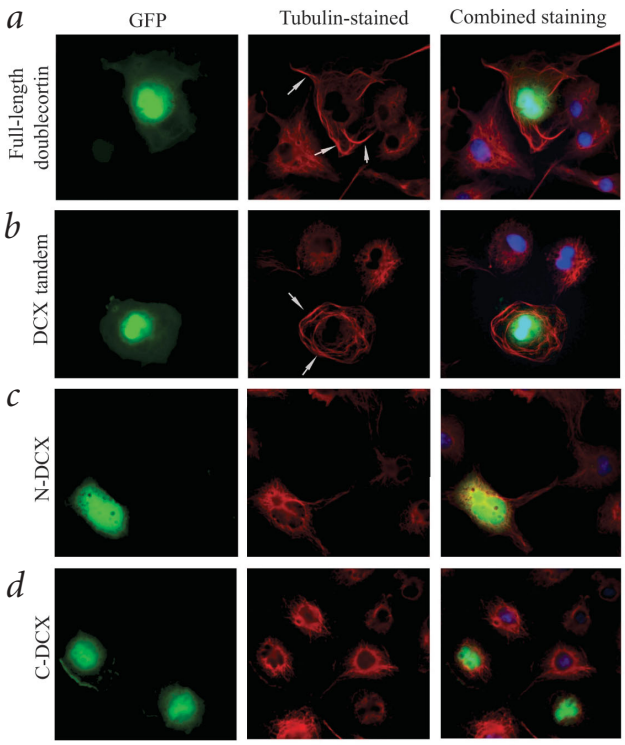

Fig. 6 *In vivo* microtubule bundling by various doublecortin fragments. ***a***, Full-length doublecortin; ***b***, DCX-tandem; ***c***, N-DCX; and ***d***, C-DCX were co-transfected into COS-7 cells together with GFP used as an independent transfection marker. The cells were visualized for GFP (green), microtubules (red) and nuclei (blue); white arrows indicate microtubule bundling.

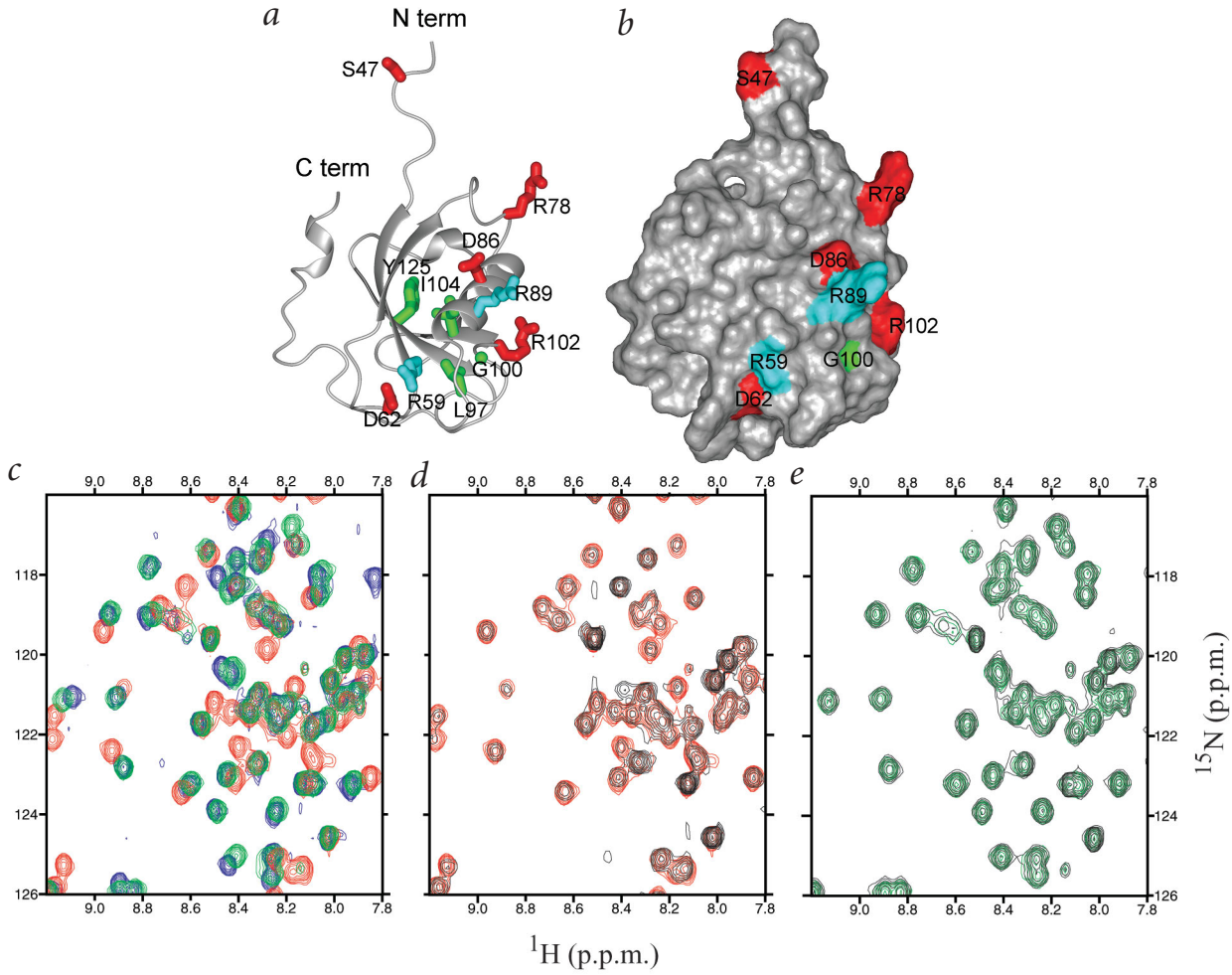

Fig. 7 Impact of two patient mutations on the structure and function of N-DCX. ***a***, The distribution of patient mutations in N-DCX shown using a ribbon representation. ***b***, A surface representation of the distribution of patient mutations. Cyan denotes the two mutants studied in this work (Arg59 and Arg89), green denotes buried sites (including partly exposed Gly100), and red denotes exposed surface residues. ***c***, Superposition of ^{1}H-^{15}N spectra of wild type N-DCX (blue), R59L N-DCX (red) and R89G N-DCX (green). ***d***, ^{1}H-^{15}N HSQC spectra of 60 μM R59L N-DCX in the presence (black) and absence (red) of equimolar polymerized tubulin at 35 °C. ***e***, ^{1}H-^{15}N HSQC spectra of 60 μM R89G N-DCX in the presence (black) and absence (green) of equimolar polymerized tubulin at 35 °C.

the NMR experiments), we used a light scattering assay. As reported with lower molar ratios[11], full-length doublecortin and the DCX tandem significantly enhanced the rate of tubulin polymerization, whereas isolated domains had a much smaller effect (data not shown).

The DCX tandem and microtubule bundling

Overexpression *in vivo* of proteins containing the DCX tandem leads to tubulin polymerization and microtubule bundling[14,32]. Because both individual DCX domains of doublecortin show the ability to bind to tubulin and/or microtubules, we wanted to explore the extent to which the tandem structure is important for the biological function.

We transfected COS-7 cells with mammalian expression vectors containing various fragments of doublecortin, followed downstream by an internal ribosome entry site and the green fluorescent protein (GFP) gene. Thus, the impact on the cytoskeleton would result exclusively from the presence of doublecortin fragments, as GFP was not a fusion partner. Although overexpression of full-length doublecortin and of the DCX tandem resulted in many cells displaying visible bundling of microtubules, little bundling was observed in cells with either N-DCX or C-DCX expressed separately (Fig. 6).

The impact of pathogenic mutations

The availability of the three-dimensional structure of the N-DCX domain, and the NMR methodology developed to assess the binding of doublecortin and its fragments to tubulin, allow us to rationalize the impact of known mutations associated with the XLIS and SBH diseases[36]. On the basis of the structural context, the mutations located in N-DCX fall, in general terms, into two categories: those likely to destabilize or affect the doublecortin structure, thereby indirectly affect its ability to interact with the tubulin cytoskeleton, and those that directly impact interactions with microtubule cytoskeleton by modifying the relevant surface epitopes (Fig. 7*a*,*b*).

The first group of mutations is likely to include mostly buried sites and sites with a distinct structural role. Three such sites are the buried, Leu97, Ile 104 and Tyr125, with the corresponding mutants (with the mutant-related syndrome indicated in parentheses) — L97R (SBH), I104T (SBH), Y125H (XLIS) and Y125D (SBH) — almost certainly leading to a loss of or reduction in sta-

Table 1 Statistics of the final CNS refined structure of N-DCX

Number of restraints	
Unambiguous distance restraints (all)	1,490
Intraresidual	390
Sequential	431
Medium range	232
Long range	437
Ambiguous distance restraints[1]	202 (459)
Hydrogen bonds	18
ϕ / ψ angle restraints	36
χ_1 angle restraints	34
$^3J_{HN\alpha}$ coupling constants	93
R.m.s. deviations from experimental restraints	
Unambiguous distance restraints (Å)	0.018 ± 0.001
Ambiguous distance restraints (Å)	0.009 ± 0.001
Hydrogen bond restraints (Å)	0.023 ± 0.003
Dihedral angle restraints (°)	0.61 ± 0.036
Coupling constants (Hz)	0.46 ± 0.020
Deviations from idealized covalent geometry	
Bonds (Å)	0.0024 ± 0.00006
Angles (°)	0.366 ± 0.005
Impropers (°)	0.524 ± 0.007
Measures of structure quality (Ramachandran plot) (%)[2]	
Residues in most favored regions	76.8 (83.6)
Residues in additional allowed regions	19.5 (14.7)
Residues in generously allowed regions	2.4 (1.2)
Residues in disallowed regions	1.3 (0.6)
Pairwise r.m.s. deviation (Å)[3]	
Backbone (N, Cα, C, O)	0.64 ± 0.08
All heavy atoms	1.35 ± 0.11

[1]Value in parentheses for this entry indicates total number of assignments.
[2]Structure quality was evaluated by PROCHECK[54] for two models: the complete domain (residues 52–146) and the core domain lacking partially folded C-terminus (residues 52–129; in parentheses).
[3]Pairwise r.m.s. deviations are calculated between 20 conformers for residues 52–146.

bility. Residue Gly100 is in a conformation disallowed for residues other than Gly; therefore; its substitution to Ala in XLIS is also potentially destabilizing. At least two patient mutations are found in position 59: R59H (SBH) and R59L[10]. This site is located near the carboxyl end of strand β1, and most of the Arg side chain atoms are buried. The guanidinium group is sequestered between Asp62 and Asp93, serving as an electrostatic zipper. The arginine in this position is conserved in all DCX domains, attesting to its functional importance. The D62N mutation is also pathogenic, leading to XLIS, probably for similar reasons. The second group of missense mutations appears to affect the electrostatic potential on the surface of the domain. They are S47R (XLIS), R78L (SBH), R78H (SBH), D86H (SBH), R89G (SBH) and R102S (XLIS).

To verify experimentally our thesis about two different classes of mutations, we studied two mutants of N-DCX previously shown to have impaired tubulin polymerization properties[11]: R59L (potential destabilization of the structure) and R89G (localized surface charge distribution). The ^{1}H-^{15}N HSQC spectra of the R59L mutant show severe structural changes, as judged by the extensive and substantial chemical shift changes relative to the wild type spectra (Fig. 7*c*). In the presence of polymerized tubulin, there is a limited degree of broadening substantially less than that observed for wild type, suggesting that this mutant may have a binding activity that is significantly impaired (Fig. 7*d*). In contrast, the R89G mutation does not affect the structure (Fig. 7*c*) but fails to bind polymerized tubulin, as judged by the lack of any broadening in the presence of tubulin (Fig. 7*e*), indicating that Arg89 contributes critical interactions for binding to microtubules. Although the sample of mutants in the current study is limited, the experimental data confirm the expected impact of mutation. The NMR methodology used in our experiments offers the advantage of clear discrimination of direct impact of the mutation on the interaction with tubulin from indirect effects caused by structural perturbations.

The homology-based model of C-DCX also allowed for a qualitative assessment of the patient mutations that occur in that domain. There are mutations clearly affecting buried sites, such as I214T (SBH), V236I (SBH), I250N (SBH) and I250T (SBH), and these may affect the structure. The mutation R186C (SBH) corresponds to R59L in N-DCX, and the consequences of the two mutations should be similar. Other mutations are more likely to change the distribution of the surface charge: P191R (SBH), P191L (SBH), R192W (XLIS), R196H (XLIS), N200K (SBH), N200I (SBH), T203A (SBH), T203R (XLIS), T222I (SBH), G223E (SBH) and G253D (SBH). Because MAPs in general are known for their relatively high isoelectric points that are key to the electrostatic interactions with negatively charged tubulin, these specific mutations in doublecortin may directly impact on its interactions with either tubulin or microtubules.

Concluding remarks

We have provided extensive structural characterization of a new class of microtubule-interacting domains, occurring typically in tandem. Although many of our functional results are consistent with those published, some are in disagreement. The most important difference is in our observation that the N-terminal DCX domain of doublecortin cannot bind to soluble tubulin, in contrast to other reports[11]. However, we obtained this result by two independent techniques, a pull-down assay with biotinylated tubulin and NMR, with consistent results. We note that unlike other reported studies, our experiments were conducted with untagged proteins, precisely corresponding to the functional domains, and by monitoring binary interactions that are free of additional reagents. These differences may explain the discrepancies, and the present results are probably closer to the physiological conditions.

With the structural results in hand, it is tempting to speculate as to the general scheme by which doublecortin, and perhaps other proteins containing the DCX-tandem, enhances tubulin polymerization and bundling. With one domain that interacts with the tubulin dimer and one that is specific for microtubules, one can envision that the enhanced polymerization of tubulin, mediated by doublecortin, results from its action as a nucleation catalyst. In this mechanism, formation of nascent microtubules will be stabilized by the tethering of tubulin dimers to one another by doublecortin. On the other hand, the observed bundling effect can be envisioned to result from doublecortin acting as a crosslinking agent between microtubules.

Methods

Protein expression and purification. The DNA encoding full-length human doublecortin was amplified by PCR and re-subcloned into *Nco*I and *Eco*RI sites of pGSTUni1 expression vector[37]. The DCX tandems of doublecortin (residues 45–275) and DCLK (residues 49–280) were subcloned into the *Eco*RI and the *Hin*dIII sites of the pHisUni1 expression vector[37]. The DNA fragments coding for N-DCX

Table 2 Crystallographic data

	SeMet inflection λ2	SeMet peak λ1	SeMet remote λ3	Native λ4
Data collection				
Wavelength	0.9795	0.9791	0.9718	0.9187
Resolution (Å)[1]	1.6 (1.66–1.6)	1.6 (1.66–1.6)	1.6 (1.66–1.6)	1.5 (1.55–1.5)
Number of reflections				
Total	28,275	28,259	29,160	47,701
Unique	9,312	8,997	9,217	15,460
Redundancy	3.0	3.1	3.2	3.1
Completeness (%)[1]	84.6 (35.9)	81.9 (10.1)	83.7 (17.7)	96.8 (85.7)
R_{sym} (%)[1,2]	3.8 (21.0)	4.2 (21.4)	3.2 (15.0)	8.4 (28.6)
$I / \sigma (I)$	32.5 (3.2)	31.0 (4.3)	41.7 (5.3)	14.1 (2.5)
Phasing statistics				
Phasing power (iso / ano)[3]	– / 2.1	0.37 / 2.1	0.98 / 1.9	
R_{cullis} (iso / ano)[4]	– / 0.64	0.77 / 0.64	0.56 / 0.68	
Refinement statistics				
Model composition				
Residues	106			111
Sulfate ions	2			2
Water	138			190
Resolution limits (Å)	10–1.6			20–1.5
Reflections				
Working set	8,418			14,683
Test set	838			770
R-factor[5]	12.7			15.3
R_{free} (%)[5]	18.0			18.7
R.m.s. deviation				
Bond (Å)	0.016			0.016
Angle (°)	1.5			1.7
Ramachandran plot (residues / %)				
Most favored regions	84 / 89.4			79 / 88.8
Additional allowed regions	10 / 10.6			10 / 11.2
Generously allowed regions	0 / 0.0			0 / 0.0
Disallowed regions	0 / 0.0			0 / 0.0

[1]The numbers in parentheses describe the relevant value for the last resolution shell.
[2]$R_{sym} = \Sigma |I_i - \langle I \rangle| / \Sigma I$, where I_i is the intensity of the i^{th} observation and $\langle I \rangle$ is the mean intensity of the reflections. The values for data collected from SeMet crystal are for unmerged Friedel pairs.
[3]Phasing power = r.m.s. ($|F_h| / E$), where $|F_h|$ is the heavy atom structure factor amplitude and E is residual lack of closure error.
[4]$R_{cullis} = \Sigma||F_{ho}| - ||F_{hc}|| / \Sigma|F_h|$ for acentric reflections, where $|F_{ho}|$ is the observed heavy atom structure factor amplitude and $|F_{hc}|$ is the calculated heavy atom structure factor amplitude.
[5]*R*-factor = $\Sigma||F_o| - |F_c|| / \Sigma|F_o|$, the crystallographic *R*-factor, and $R_{free} = \Sigma||F_o| - |F_c|| / \Sigma|F_o|$, where all reflections belong to a test set of randomly selected data.

(residues 45–150), C-DCX (residues 170–275), N-DCLK (residues 49–154) and C-DCLK (residues 176–280) were subcloned into the *Eco*RI and the *Xba*I sites of pGSTUni1 vector. The C-terminally truncated N-DCX (residues 45–141) was created from N-DCX as template using QuikChange site-directed mutagenesis (Stratagene) by the two-stage PCR method[38]. The R59L and R89G mutants of N-DCX and the L120M mutant of N-DCLK were generated using QuikChange. Protein production in *E. coli* BL21(DE3) cells (Novagen) carrying the plasmids was induced by the addition of 1 mM IPTG (Sigma) in LB medium at 20 °C. The N-DCLK (L120M) plasmid was used to transform the methionine auxotroph *E. coli* B834(DE3) (Novagen), and expression was carried out using minimal medium supplemented with 50 mg ml^{-1} SeMet (Sigma). The constructs have a seven-residue cloning artifact (GAMDPQF) at the N terminus, except for the L120M mutant (which has a single Gly) and the full length doublecortin (which has additional Gly-Ala). Uniformly $^{15}N/^{13}C$- and ^{15}N-labeled proteins were overexpressed in a minimal medium containing $(^{15}NH_4)_2SO_4$ either with or without $^{13}C_6$-glucose, respectively. The full-length doublecortin was purified by glutathione affinity chromatography (Pharmacia) followed by the removal of GST by rTEV protease (Gibco) and NaCl gradient elution from Resource 30S chromatography (Pharmacia). N-DCX, C-DCX, the truncated N-DCX, N-DCLK, C-DCLK and the SeMet-substituted mutant were purified by glutathione affinity chromatography, followed by the removal of GST by rTEV protease and gel filtration chromatography (Superdex 75, Pharmacia). The DCX-tandems of doublecortin and DCLK were purified by Ni-affinity chromatography (Qiagen) followed by the removal of the His_6-tag by rTEV protease and gel filtration.

NMR spectroscopy. NMR spectra were measured on Varian Inova 500 and 800 MHz NMR spectrometers, as well as a cryoprobe-equipped Bruker DRX 500 MHz NMR spectrometer. Protein samples prepared for structure determination contained 1 mM ^{15}N- or $^{13}C/^{15}N$-labeled N-DCX in 50 mM phosphate buffer, pH 6.0, 5 mM DTT and 10% D_2O. Studies of interactions of DCX domains with tubulin (Cytoskeleton) were typically carried out at 1:1 molar ratio at 60 μM concentrations. Protein samples were dissolved in 80 mM PIPES, 1 mM EGTA and 1 mM $MgCl_2$ (PEM buffer, Cytoskeleton), pH 6.8, supplemented with 1 mM GTP and 10% D_2O. Samples were prepared on ice and ^1H-^{15}N HSQC spectra were measured at two temperatures: 20 °C (unpolymerized tubulin) and 35 °C (polymerized tubulin).

N-DCX solution structure determination. NMR spectra used for assignment and structure determination of N-DCX were measured at 25 °C. Three NOESY spectra with 100 ms mixing times were used to determine distance restraints: ^{15}N-edited NOESY and two ^{13}C-edited NOESY spectra for aliphatic and aromatic carbon sweep widths, respectively. Spectra were processed and analyzed with NMRPipe[39] and SPARKY[40]. NOESY crosspeaks were assigned using a combination of manual and automatic assignment using NOAH/DYANA[41]. The final set of structures was refined with CNS[42] using distance restraints supplemented with ϕ, ψ angle restraints for regular secondary structures generated using TALOS[43], $^3J_{HNH\alpha}$ coupling constants, χ_1 dihedral angle restraints for stereospecifically assigned residues and restraints for interstrand hydrogen bonds. NOE crosspeaks with multiple assignment possibilities were used as ambiguous distance restraints[44]. The 20 lowest energy conformers were used for the analysis.

Crystallization. The crystallization of the N-DCLK and SeMet-substituted N-DCLK (L120M) is described in detail elsewhere[45]. Briefly, the native crystals were grown by sitting drop vapor diffusion at 21 °C by mixing equal volumes of protein solution (10 mg ml^{-1}) and reservoir solution (1.8–2.0 M $(NH_4)_2SO_4$ and 0.1 M Na_3-citrate, pH 5.0) and used as a seed for the mixed drop solution of equal volumes of protein solution (5 mg ml^{-1}) and reservoir solution containing 1.55 M $(NH_4)_2SO_4$ and 0.1 M Na_3-citrate, pH 5.0. Single, plate-like crystals were allowed to grow for three months. The SeMet-substituted protein crystals of N-DCLK (L120M) were grown by sitting drop vapor diffusion at 21 °C by mixing equal volumes of 15 mg ml^{-1} protein and reservoir solution that contained 2.2–2.4 M $(NH_4)_2SO_4$ and 0.1 M Na_3-citrate, pH 5.2–5.8. Plate-like cluster crystals took about two weeks to grow.

X-ray data collection. All data sets were collected at 100 K. The crystals were frozen using 30% (w/v) glycerol in the mother liquor as a cryo-protectant. Native data were collected from a monoclinic crystal in the *C*2 space group, with the cell dimensions of a = 85.98 Å, b = 29.62 Å, c = 40.33 Å and β = 101.3°. Data were collected at SBC 19ID beamline at Advanced Photon Source synchrotron to 1.5 Å resolution. SeMet crystals were also monoclinic, but belonged to space group $P2_1$ with a = 38.81 Å, b = 29.43 Å, c = 40.10 Å and β = 115.7°. MAD data (three wavelengths) were collected at X9B beamline of the NSLS (Brookhaven National Laboratory) to 1.6 Å resolution. All data were processed with the HKL2000 package[46] (Table 2).

Crystal structure determination. Anomalous differences from the selenium edge data set were used for initial location of the single Se atom using direct methods in SHELXS[47]. Phase refinement was carried out with MLPHARE from the CCP4 suite[48] and SHARP[49]. Following density modification with SOLOMON[50], the experimental electron density map was used for automated model building with ARP/wARP[51], which built 100 out of 106 residues. The refinement was carried out using REFMAC5 (ref. 52) with anisotropic *B*-factor refinement option in the final stage. We solved the monoclinic *C*2 crystal structure by molecular replacement with AMoRe[53] using the partially refined model of the $P2_1$ crystal form. The structure was refined with REFMAC5 using anisotropic *B*-factors. The model in this crystal form contains 111 residues, 2 sulfate ions and 190 water molecules. Both $P2_1$ and *C*2 models satisfy or exceed the quality criteria limits of PROCHECK[54].

Stability studies. Thermal denaturations were performed on a J-715 spectropolarimeter (Jasco) following the ellipticity at 220 nm and a 2 nm bandwidth with a response time of 4 s in 25 mM Tris and 300 mM NaCl, pH 7.0, at 1 °C min^{-1} heating rate. Protein concentration was 15–50 μg ml^{-1}. Analysis of the data was performed using PeakFit software (Jandel Scientific Software). Solvent denaturations were performed on a FP-750 spectrofluorimeter (Jasco) or J-715 spectropolarimeter (Jasco) at 21 °C. Protein samples in various concentrations of guanidine-HCl in 25 mM Tris, pH 7.0, were equilibrated for 24 h at 21 °C. The transitions were monitored by the decrease of the CD signal at 220 nm at 2 nm bandwidth or decrease of fluorescence at 348 nm on excitation at 280 nm with 5 nm emission and excitation bandwidths. The apparent free-energy change in the absence of guanidine-HCl (ΔG_{den}) was determined by fitting the ellipticity or fluorescence intensity changes at particular concentrations of guanidine-HCl to the equation given by Santoro and Bolen[55].

ANS binding. The binding of ANS was measured on a FP-750 spectrofluorimeter (Jasco) at 21 °C in 25 mM Tris and 300 mM NaCl, pH 7.0. Emission spectra of 20 mM ANS on excitation at 350 nm were collected after 20 min of incubation with protein.

Hydrodynamic properties. Gel filtration performed on Superdex 75 analytical column (Amersham Pharmacia) equilibrated with 25 mM Tris, pH 7.0, and 300 mM NaCl. Samples of 100 μl were eluted at a flow rate 0.2 ml min^{-1}, and the absorption of the eluent was recorded at 215 nm using ÄKTA FPLC (Amersham Pharmacia). The hydrodynamic radius (R_s) for doublecortin and DCLK and their domains were calculated from a linear dependence of R_s values *versus* elution volume determined for standard proteins.

Pull-down assays. *In vitro* tubulin binding assay was performed in a buffer containing 100 mM NaCl, 50 mM Tris, pH 7.4, 5 mM EDTA and 0.07% (w/v) Triton X-100. Biotin-conjugated tubulin at 10 μg ml^{-1} (Cytoskeleton) was mixed with full-length doublecortin (0.1 μg ml^{-1}), DCX tandem (0.1 μg ml^{-1}), N-DCX (5 μg ml^{-1}) and C-DCX (3 μg ml^{-1}) in 0.5 ml binding buffer containing 15 μl avidin resin (Promega). A set of samples that contained the same amount of protein and avidin resin, but without biotynilated tubulin, was used as a negative control. The binding mixture was incubated at 4 °C with gentle rotation for 3 h. Proteins bound to the avidin resin were pelleted down, washed 5× in the binding buffer and eluted with SDS-PAGE sample buffer at 95 °C. The protein bound either from supernatant or the pellet was analyzed by 13% SDS-PAGE, followed by immunoblotting with polyclonal antibodies to doublecortin and /or tubulin.

***In vivo* assays using COS-7 cells.** COS-7 cells were grown in monolayer on cover glass before being transfected with DCX constructs cloned in pIRES-hrGFP-1a vector (Stratagene). Transfection was performed using lipofectamine (Invitrogen) according to manufacturer's instructions. Cells were fixed ~48 h later with 4% formaldehyde in PBS (phosphate buffered saline, 138 mM NaCl and 2.7 mM KCl, pH 7.4) and stained in PBS containing 0.1% (w/v) Triton X-100 with monoclonal antibody to tubulin B-5-1 (Sigma) followed by rhodamine-conjugated anti-mouse to view microtubules. Hoechst 33342 was used to visualize nuclear DNA. The cells were examined with an Olympus microscope equipped for epifluorescence.

Coordinates. The coordinates have been deposited in the Protein Data Bank (accession codes 1MFW for the SeMet-labeled N-DCLK L120M mutant, 1MG4 for the native N-DCLK and 1MJD for the NMR-derived coordinates of N-DCX).

Acknowledgments

This research is supported by NIH grants to Z.S.D. and to C.A.W. A NATO Collaborative Link grant to Z.S.D. and J.O. is gratefully acknowledged. T.C. and D.K. are recipients of the Young Scholar Awards from the Foundation for Polish Science. J.O. is an International Scholar of the Howard Hughes Medical Institute. J.H.B. is supported by grants from the NIH and the Leukemia and Lymphoma Society. We thank N. Olekhnovich for excellent technical assistance, F. Abildgaard of NMRFAM for assistance with the collection of some of the NMR data, P. Sheffield for his contribution in the early phase of the project, A.V. Somlyo for helpful comments on the manuscript and L. Tamm for assistance with the tubulin polymerization experiments.

Competing interests statement

The authors declare that they have no competing financial interests.

Received 20 November, 2002; accepted 11 March, 2003.

1. Nogales, E. Structural insight into microtubule function. *Annu. Rev. Biophys. Biomol. Struct.* **30**, 397–420 (2001).
2. Mandelkow, E. & Mandelkow, E.M. Microtubules and microtubule-associated proteins. *Curr. Opin. Cell Biol.* **7**, 72–81 (1995).
3. Gleeson, J.G. *et al*. doublecortin, a brain-specific gene mutated in human X-linked lissencephaly and double cortex syndrome, encodes a putative signaling protein. *Cell* **92**, 63–72 (1998).
4. des Portes, V. *et al*. A novel CNS gene required for neuronal migration and involved in X-linked subcortical laminar heterotopia and lissencephaly syndrome. *Cell* **92**, 51–61 (1998).
5. Raymond, A.A. *et al*. Abnormalities of gyration, heterotopias, tuberous sclerosis, focal cortical dysplasia, microdysgenesis, dysembryoplastic neuroepithelial tumour and dysgenesis of the archicortex in epilepsy. Clinical, EEG and neuroimaging features in 100 adult patients. *Brain* **118**, 629–660 (1995).
6. Francis, F. *et al*. doublecortin is a developmentally regulated, microtubule-associated protein expressed in migrating and differentiating neurons. *Neuron* **23**, 247–256 (1999).
7. Gleeson, J.G., Lin, P.T., Flanagan, L.A. & Walsh, C.A. doublecortin is a microtubule-associated protein and is expressed widely by migrating neurons. *Neuron* **23**, 257–271 (1999).
8. Dobyns, W.B. & Truwit, C.L. Lissencephaly and other malformations of cortical development: 1995 update. *Neuropediatrics* **26**, 132–147 (1995).
9. Dobyns, W.B., Reiner, O., Carrozzo, R. & Ledbetter, D.H. Lissencephaly. A human brain malformation associated with deletion of the LIS1 gene located at chromosome 17p13. *J. Am. Med. Assoc.* **270**, 2838–2842 (1993).
10. Sapir, T. *et al*. doublecortin mutations cluster in evolutionarily conserved functional domains. *Hum. Mol. Genet.* **9**, 703–712 (2000).
11. Taylor, K.R., Holzer, A.K., Bazan, J.F., Walsh, C.A. & Gleeson, J.G. Patient mutations in doublecortin define a repeated tubulin-binding domain. *J. Biol. Chem.* **275**, 34442–34450 (2000).
12. Burgess, H.A. & Reiner, O. doublecortin-like kinase is associated with microtubules in neuronal growth cones. *Mol. Cell. Neurosci.* **16**, 529–541 (2000).
13. Burgess, H.A., Martinez, S. & Reiner, O. KIAA0369, doublecortin-like kinase, is expressed during brain development. *J. Neurosci. Res.* **58**, 567–575 (1999).
14. Lin, P.T., Gleeson, J.G., Corbo, J.C., Flanagan, L. & Walsh, C.A. DCAMKL1 encodes a protein kinase with homology to doublecortin that regulates microtubule polymerization. *J. Neurosci.* **20**, 9152–9161 (2000).
15. Schultz, J., Copley, R.R., Doerks, T., Ponting, C.P. & Bork, P. SMART: a web-based tool for the study of genetically mobile domains. *Nucleic Acids Res.* **28**, 231–234 (2000).
16. Gonczy, P. *et al*. *zyg-8*, a gene required for spindle positioning in *C. elegans*, encodes a doublecortin-related kinase that promotes microtubule assembly. *Dev. Cell* **1**, 363–375 (2001).
17. Sullivan, L.S. *et al*. Mutations in a novel retina-specific gene cause autosomal dominant *retinitis pigmentosa*. *Nat. Genet.* **22**, 255–259 (1999).
18. Cierpicki, T., Kim, M.H., Otlewski, J., Derewenda, Z.S. & Bushweller, J.H. Assignment of ^{1}H, ^{13}C and ^{15}N resonances of the N-terminal microtubule-binding domain of human doublecortin. *J. Biomol. NMR* **25**, 81–82 (2003).
19. Holm, L. & Sander, C. Protein structure comparison by alignment of distance matrices. *J. Mol. Biol.* **233**, 123–138 (1993).
20. Huang, L., Hofer, F., Martin, G.S. & Kim, S.H. Structural basis for the interaction of Ras with RalGDS. *Nat. Struct. Biol.* **5**, 422–426 (1998).
21. Ito, T., Matsui, Y., Ago, T., Ota, K. & Sumimoto, H. Novel modular domain PB1 recognizes PC motif to mediate functional protein–protein interactions. *EMBO J.* **20**, 3938–3946 (2001).
22. Terasawa, H. *et al*. Structure and ligand recognition of the PB1 domain: a novel protein module binding to the PC motif. *EMBO J.* **20**, 3947–3956 (2001).
23. Buchberger, A., Howard, M.J., Proctor, M. & Bycroft, M. The UBX domain: a widespread ubiquitin-like module. *J. Mol. Biol.* **307**, 17–24 (2001).
24. Vijay-Kumar, S., Bugg, C.E. & Cook, W. J. Structure of ubiquitin refined at 1.8 Å resolution. *J. Mol. Biol.* **194**, 531–544 (1987).
25. Scheffzek, K. *et al*. The Ras-Byr2RBD complex: structural basis for Ras effector recognition in yeast. *Structure* **9**, 1043–1050 (2001).
26. Uversky, V.N. Natively unfolded proteins: a point where biology waits for physics. *Protein Sci.* **11**, 739–756 (2002).
27. Semisotnov, G.V. *et al*. Study of the "molten globule" intermediate state in protein folding by a hydrophobic fluorescent probe. *Biopolymers* **31**, 119–128 (1991).
28. Itzhaki, L.S., Evans, P.A., Dobson, C.M. & Radford, S.E. Tertiary interactions in the folding pathway of hen lysozyme: kinetic studies using fluorescent probes. *Biochemistry* **33**, 5212–5220 (1994).
29. Engelhard, M. & Evans, P.A. Kinetics of interaction of partially folded proteins with a hydrophobic dye: evidence that molten globule character is maximal in early folding intermediates. *Protein Sci.* **4**, 1553–1562 (1995).
30. Eliezer, D. & Wright, P.E. Is apomyoglobin a molten globule? Structural characterization by NMR. *J. Mol. Biol.* **263**, 531–538 (1996).
31. Kitahara, R., Yamada, H., Akasaka, K. & Wright, P.E. High pressure NMR reveals that apomyoglobin is an equilibrium mixture from the native to the unfolded. *J. Mol. Biol.* **320**, 311–319 (2002).
32. Horesh, D. *et al*. doublecortin, a stabilizer of microtubules. *Hum. Mol. Genet.* **8**, 1599–1610 (1999).
33. Yoshiura, K., Noda, Y., Kinoshita, A. & Niikawa, N. Colocalization of doublecortin with the microtubules: an *ex vivo* colocalization study of mutant doublecortin. *J. Neurobiol.* **43**, 132–139 (2000).
34. Fygenson, D.K., Flyvbjerg, H., Sneppen, K. & Libchaber, A. Spontaneous nucleation of microtubules. *Phys. Rev. E* **51**, 5058–5063 (1995).
35. Fygenson, D.K., Braun, E. & Libchaber, A. Phase diagram of microtubules. *Phys. Rev. E* **50**, 1579–1588 (1994).
36. Krawczak, M. & Cooper, D.N. The human gene mutation database. *Trends Genet.* **13**, 121–122 (1997).
37. Sheffield, P., Garrard, S. & Derewenda, Z. Overcoming expression and purification problems of RhoGDI using a family of 'parallel' expression vectors. *Protein Expr. Purif.* **15**, 34–39 (1999).
38. Wang, W. & Malcolm, B.A. Two-stage PCR protocol allowing introduction of multiple mutations, deletions and insertions using QuikChange site-directed mutagenesis. *Biotechniques* **26**, 680–682 (1999).
39. Delaglio, F., Kontaxis, G. & Bax, A. Protein structure determination using molecular replacement and NMR dipolar couplings. *J. Am. Chem. Soc.* **122**, 2142–2143 (2000).
40. Goddard, T.D. & Kneller, D.G. SPARKY 3 (University of California, San Francisco; 2002).
41. Güntert, P., Mumenthaler, C. & Wüthrich, K. Torsion angle dynamics for NMR structure calculation with the new program DYANA. *J. Mol. Biol.* **273**, 283–298 (1997).
42. Brunger, A.T. *et al*. Crystallography & NMR system: a new software suite for macromolecular structure determination. *Acta Crystallogr. D* **54**, 905–921 (1998).
43. Cornilescu, G., Delaglio, F. & Bax, A. Protein backbone angle restraints from searching a database for chemical shift and sequence homology. *J. Biomol. NMR* **13**, 289–302 (1999).
44. Nilges, M., Macias, M.J., O'Donoghue, S.I. & Oschkinat, H. Automated NOESY interpretation with ambiguous distance restraints: the refined NMR solution structure of the pleckstrin homology domain from β-spectrin. *J. Mol. Biol.* **269**, 408–422 (1997).
45. Kim, M.H., Derewenda, U., Devedjiev, Y., Dauter, Z. & Derewenda, Z.S. Purification and crystallization of the N-terminal domain from the human doublecortin-like kinase. *Acta Crystallogr. D* **59**, 502–505 (2003).
46. Otwinowski, Z. & Minor, W. Processing of X-ray diffraction data collected in oscillation mode. *Methods Enzymol.* **276**, 307–326 (1997).
47. Sheldrick, G.M. & Gould, R.O. Structure solution by iterative peaklist optimisation and tangent expansion in space group *P*1. *Acta Crystallogr. B* **51**, 423–431 (1995).
48. Collaborative Computational Project, Number 4. The CCP4 suite: programs for protein crystallography. *Acta Crystallogr. D* **50**, 760–763 (1994).
49. Fortelle, E.D.L. & Bricogne, G. Maximum-likelihood heavy atom parameter refinement for multiple isomorphous replacement and multiwavelength anomalous diffraction methods. *Methods Enzymol.* **276**, 472–494 (1997).
50. Abrahams, J.P. & Leslie, A.G.W. Methods used in the structure determination of bovine mitochondrial F1 ATPase. *Acta Crystallogr. D* **52**, 30–42 (1996).
51. Perrakis, A., Morris, R. & Lamzin, V.S. Automated protein model building combined with iterative structure refinement. *Nat. Struct. Biol.* **6**, 458–463 (1999).
52. Murshudov, G.N., Vagin, A.A. & Dodson, E.J. Refinement of macromolecular structures by the maximum-likelihood method. *Acta Crystallogr. D* **53**, 240–255 (1997).
53. Navaza, J. AMoRE: an automated package for molecular replacement. *Acta Crystallogr. A* **50**, 157–163 (1994).
54. Laskowski, R.A., McArthur, M.W., Moss, D.S. & Thornton, J.M. PROCHECK: a program to check the stereochemical quality of protein structures. *J. Appl. Crystallogr.* **26**, 282–291 (1993).
55. Santoro, M.M. & Bolen, D.W. A test of the linear extrapolation of unfolding free energy changes over an extended denaturant concentration range. *Biochemistry* **31**, 4901–4907 (1992).